ARTICLE

Check for updates

The obligate intracellular bacterium *Orientia tsutsugamushi* differentiates into a developmentally distinct extracellular state

Sharanjeet Atwal[1,8], Jantana Wongsantichon[2,8], Suparat Giengkam[2,8], Kittirat Saharat[1], Yanin Jaiyen Pittayasathornthun[2], Suthida Chuenklin[1,2], Loo Chien Wang[3,4], Taerin Chung[5], Hyun Huh[5], Sang-Hyuk Lee[5,6], Radoslaw M. Sobota[3,4] & Jeanne Salje[1,2,7✉]

Orientia tsutsugamushi (Ot) is an obligate intracellular bacterium in the family Rickettsiaceae that causes scrub typhus, a severe mite-borne human disease. Its mechanism of cell exit is unusual amongst Rickettsiaceae, as Ot buds off the surface of infected cells enveloped in plasma membrane. Here, we show that Ot bacteria that have budded out of host cells are in a distinct developmental stage compared with intracellular bacteria. We refer to these two stages as intracellular and extracellular bacteria (IB and EB, respectively). These two forms differ in physical properties: IB is both round and elongated, and EB is round. Additionally, IB has higher levels of peptidoglycan and is physically robust compared with EB. The two bacterial forms differentially express proteins involved in bacterial physiology and host-pathogen interactions, specifically those involved in bacterial dormancy and stress response, and outer membrane autotransporter proteins ScaA and ScaC. Whilst both populations are infectious, entry of IB Ot is sensitive to inhibitors of both clathrin-mediated endocytosis and macropinocytosis, whereas entry of EB Ot is only sensitive to a macropinocytosis inhibitor. Our identification and detailed characterization of two developmental forms of Ot significantly advances our understanding of the intracellular lifecycle of an important human pathogen.

[1] Public Health Research Institute, Rutgers the State University of New Jersey, Newark, NJ, USA. [2] Mahidol-Oxford Tropical Medicine Research Unit, Faculty of Tropical Medicine, Mahidol University, Bangkok, Thailand. [3] Functional Proteomics Laboratory, Institute of Molecular and Cell Biology, Agency for Science, Technology and Research (A*STAR), Singapore, Singapore. [4] SingMass—National Mass Spectrometry Laboratory, Institute of Molecular and Cell Biology, Agency for Science, Technology and Research (A*STAR), Singapore, Singapore. [5] Institute for Quantitative Biomedicine, Rutgers University, Piscataway, NJ, USA. [6] Department of Physics and Astronomy, Rutgers University, Piscataway, NJ, USA. [7] Centre for Tropical Medicine and Global Health, Nuffield Department of Medicine, University of Oxford, Oxford, UK. [8] These authors contributed equally: Sharanjeet Atwal, Jantana Wongsantichon, Suparat Giengkam. ✉email: jeanne.salje@ndm.ox.ac.uk

*O*rientia tsutsugamushi (Ot) is an obligate intracellular Gram-negative bacterium that causes the mite-transmitted human disease scrub typhus. This condition is one of the most severe rickettsial diseases; it is associated with a median 6% mortality in untreated patients[1]. Scrub typhus is a leading cause of severe febrile illness in the Asia-Pacific, a region containing two-thirds of the world's population. Recent reports from Latin America, the Middle East, and Africa suggest that the disease is more globally distributed[2]. Knowledge of the fundamental biology of this organism lags behind that of pathogens of equivalent prevalence and severity. Historical underestimations of Ot incidence, its classification as a biosafety level 3 pathogen, its fastidious growth in cultured cells, and the fact that it remains genetically intractable[3] likely account for the paucity of studies focused on this pathogen.

The order Rickettsiales contains two major families: Anaplasmataceae and Rickettsiaceae[4]. Members of the Anaplasmataceae, which include *Anaplasma* spp. and *Ehrlichia* spp., reside within membrane-bound vacuoles inside host cells. The developmental cycle of certain Anaplasmataceae family members is biphasic and involves switching between a noninfectious intracellular replicative form (reticulate body) and an infectious extracellular form (elementary body). While members of the Rickettsiaceae, namely *Rickettsia* spp. and Ot, do not appear to differentiate into distinct forms during their intracellular lifecycle, Ot is unique amongst the characterized Rickettsiaceae in budding off the surface of infected host cells in a manner reminiscent of enveloped viruses[5]. This observation led us to investigate whether budded Ot is in a distinct developmental stage compared with intracellular counterparts.

Ot has been shown to enter host cells using the zipper-like invasion mechanism, which is common to many Rickettsiales members[4]. This process is initiated by binding of bacterial surface adhesins to receptors expressed on mammalian cells. Adhesins such as TSA56, ScaA, and ScaC[6–8] bind to host cell fibronectin and syndecan-4; these proteins then interact with integrin α5ß1, leading to activation of intracellular signaling that culminates in actin remodeling and clathrin-mediated endocytosis[9–11]. It is important to emphasize that these studies were entirely focused on intracellular Ot, as they were performed on bacteria isolated from host cells by mechanical lysis of infected cells. However, the reentry mechanism utilized by bacteria that have budded out of cells may be influenced by the presence of an enveloping host cell membrane and/or its differentiation into a distinct state.

Here, we show that Ot exists in distinct intracellular (IB) and extracellular (EB) bacterial populations. We report the characterization of these two states in terms of their physical properties, metabolic activity, and gene expression profiles and demonstrate that they enter host cells using different mechanisms.

Results

IB and EB forms of Ot differ in physical properties and metabolic activity. Ot is typically described as a coccobacillary bacterium. Its small size and propensity to aggregate make it difficult to obtain clear images of this bacterium using conventional light microscopy. To circumvent this challenge, we labeled Ot with an antibody against the abundant surface protein TSA56 and employed stochastic optical reconstruction microscopy (STORM) for high-resolution imaging. We first investigated the shape of bacteria located inside and outside host cells (Fig. 1A, B and Supplementary Fig. 1). Since Ot begins to appear in the supernatant of infected L929 cells at high levels 5 days post-infection (Supplementary Fig. 2) we focused on the shape of EB Ot beginning 5 days post-infection, whilst we measured the shape of IB Ot throughout the infection cycle. We found that EBs were approximately round in shape with a diameter of about 1.2 μm,

and they were often aggregated into clusters. In contrast, IBs adopted diverse round and elongated shapes and varied in dimensions; some bacteria were 3–4 μm in length. Additionally, IB size varied during the course of infection. Initially, and up to 1-day post-infection, IBs were similar in length to EBs. At later stages, i.e., 2–7 days following infection, IBs were characterized by longer lengths. These kinetic changes in shape correlated with Ot growth dynamics whereby replication starts 24–48 h post-infection[12]. These differences in shape provide evidence for the existence of two separate bacterial forms.

We next investigated potential differences in bacterial cell wall composition. We previously showed that Ot builds a low-abundance peptidoglycan-like structure[13]. Thus, we assessed relative peptidoglycan levels in IB and EB Ot forms using a NOD1 reporter assay (Fig. 1C). We detected significantly more peptidoglycan in IB cells compared with EB cells. This finding may account for the observed differences in shape (Fig. 1A) as peptidoglycan is required to build elongated cells.

In related structural studies, we capitalized on our previous finding that the abundant surface protein TSA56 is involved in forming disulfide bonds with itself or other proteins, leading to the formation of aggregates[13]. These complexes can be identified as smears following sample preparation in the absence of reducing agents and evaluation by immunoblot analyses. In this study, we found evidence for substantially higher disulfide bond formation in EB Ot than IB Ot, as determined by the presence of a high molecular weight smear (Fig. 1D). We hypothesize that this crosslinked structure confers EB Ot with additional structural rigidity in the absence of peptidoglycan. These experiments were performed in the presence of iodoacetamide, an agent that covalently modifies cysteine residues and prevents them from forming new bonds, thus ensuring that the cross-links were not formed during sample preparation and processing.

Our next goal was to assess potential changes in genome copy number as, during rapid growth, bacteria such as *E. coli* carry multiple genome copies within a single cell. To address this issue, we determined bacterial cell numbers using fluorescence microscopy and bacterial genome copies using qPCR. We found no differences: Ot IB and EB harbored just over one estimated genome copy per cell (Fig. 1E). This measurement is an approximation that suffers limitations associated with absolute quantification using qPCR and microscopy, but any such errors are expected to be constant between the IB and EB measurements.

Finally, we asked whether IB and EB Ot forms differed in their metabolic activity. Ot is an obligate intracellular bacterium with limited central metabolic and biosynthetic capability[14] and a reliance on host cells for carbon and nitrogen sources and metabolic intermediates. These observations led us to hypothesize that EB bacteria are metabolically inactive owing to their extracellular location. To test this, we used a microscopy-based assay whereby growing bacteria are exposed to a clickable methionine analog L-Homopropargylglycine (HPG) that is subsequently labeled with a fluorophore[15] (Fig. 2A). Using this methodology, we observed that 95% of IB were translationally active 5 days post-infection, compared with 0% of EB (Fig. 2B). It is possible that EB Ot undergo some residual metabolic activity that is not detected by our assay of protein translation. The fact that not all IB were labeled with HPG indicated that this result did not simply reflect a difference in bacterial permeability between the IB and EB forms. These results provide an additional line of evidence to support the existence of two fundamentally different Ot states.

IB and EB forms of Ot exhibit different gene and protein expression profiles. We next investigated whether the differences
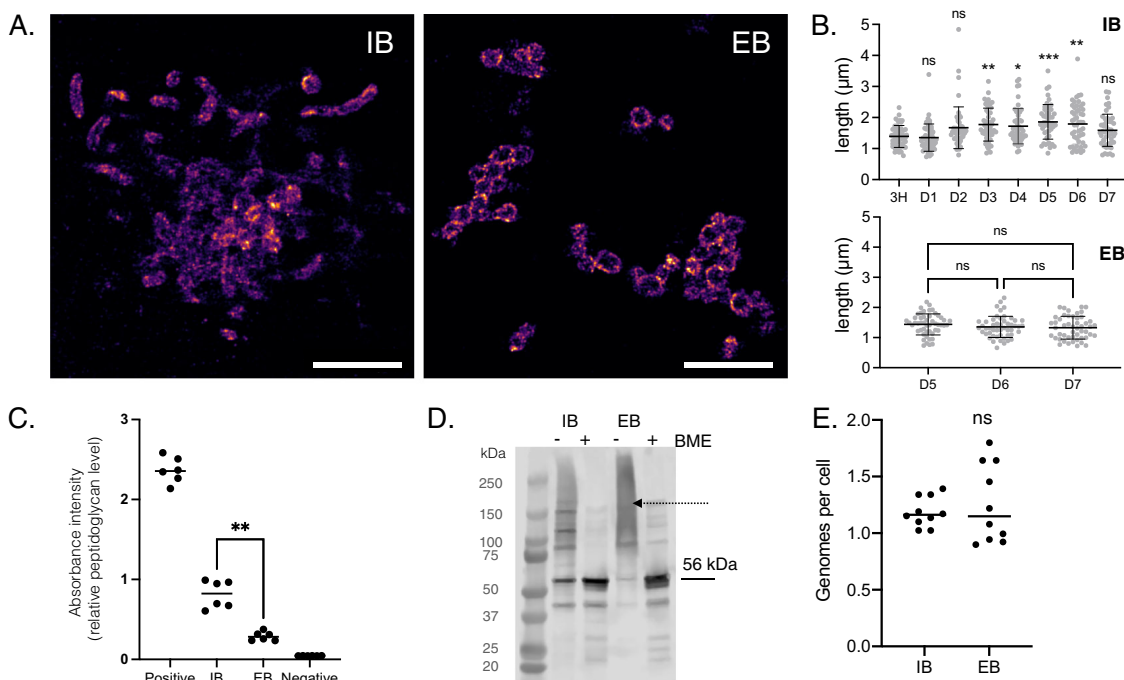
Fig. 1 Intracellular and extracellular forms of Ot are physically distinct. A Representative STORM images of IB (5 d.p.i.) and EB (7 d.p.i.) Ot in L929 cells. Bacteria were labeled with a monoclonal antibody against surface protein TSA56 (magenta). Additional images including DIC images of host cells are provided in Supplementary Fig. 1. Scale bar = 5 μm. **B** Length quantification of individual IB and EB Ot as imaged by STORM. H hours, D days post-infection. The lengths of 50 individual IB (defined as colocalising with host cells) and EB form (defined as not colocalising with host cells) Ot were measured. Statistical significance was determined using a one-way ANOVA followed by Dunnett's multiple comparisons. $n = 50$ individual bacteria from one experiment. Data are presented as mean values ± SD. **C** Quantification of relative peptidoglycan levels through activation of NOD1 reporter cells, as measured by secreted alkaline phosphatase activity. EB Ot induced less activation than IB, indicating lower levels of peptidoglycan. Identical amounts of IB and EB Ot were used, taken from L929 cells 5 days post-infection. The results of six independent replicates, carried out on two different days, are shown and the statistical significance was determined using a two-tailed Mann–Whitney test. Positive control = meso-diaminopimelic acid, negative control = PBS. $P = 0.0022$. **D** Immunoblot showing the formation of disulfide crosslinked aggregates of the surface protein TSA56, observed in the absence of the reducing agent betamercaptoethanol (BME). This effect was stronger in EB compared with IB Ot, taken 5 days post-infection from L929 cells. The expected molecular weight of TSA56 (56 kDa) is indicated with an arrow, and a dashed arrow depicts higher-order aggregates. **E** Genome copy number per cell as measured by qPCR; bacterial cell number was determined by immunofluorescence microscopy. Quantification of 10 individual imaging fields is shown, and statistical significance determined using a two-tailed Mann–Whitney test. $n = 10$ individual imaging fields from one experiment.

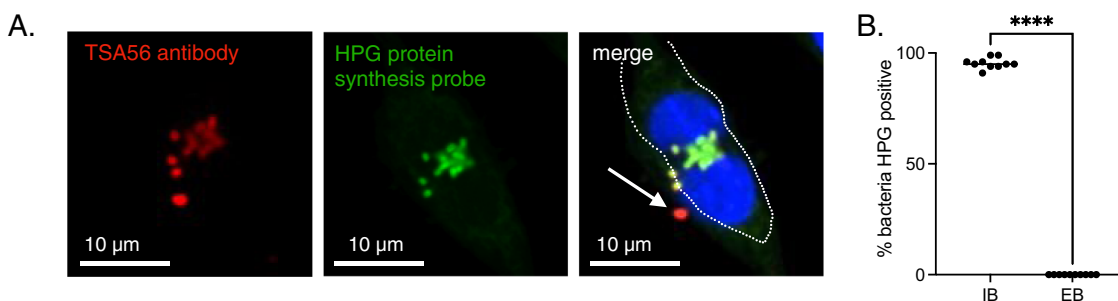**Fig. 2 Intracellular and extracellular forms of Ot are metabolically distinct. A** Confocal microscopy image of an L929 cell infected with Ot for 5 days and labeled with the clickable methionine analog homopropargylglycine (HPG, green) and an antibody against surface protein TSA56 (red). DNA (Hoechst) is shown in blue. The host cell outline is showed by a dashed line, and an arrow indicates a metabolically inactive bacterium located outside the host cell. **B** Quantification of metabolic activity, as measured by a detectable HPG signal, in IB and EB Ot. L929 cells were infected with Ot for 5 days, fixed, and labeled with TSA56 and HPG. Bacteria were identified as being IB or EB, based their position relative to host cells, and the percentage of each population that was HPG-positive was quantified. The percentage positivity for ten randomly imaged field is shown here, and this data is representative of >3 independent repeats of this experiment. Groups were compared using a two-sided Mann–Whitney test. Statistical significance for all data in this figure was determined using Graphpad Prism software. *p value ≤ 0.05, **p value ≤ 0.01, ***p value ≤ 0.001, ****p value ≤ 0.0001, ns not significant.

in physical properties and metabolic activity observed in IB and EB forms of Ot were accounted exclusively by physical location relative to host cells. Exposure of EB forms to an osmotically different extracellular environment combined with the lack of nutrient availability might account for our observations. However, a second possibility is that EB forms arise by differentiation of IB into a biochemically distinct state. We reasoned that bacteria in the same developmental stage but differing in position
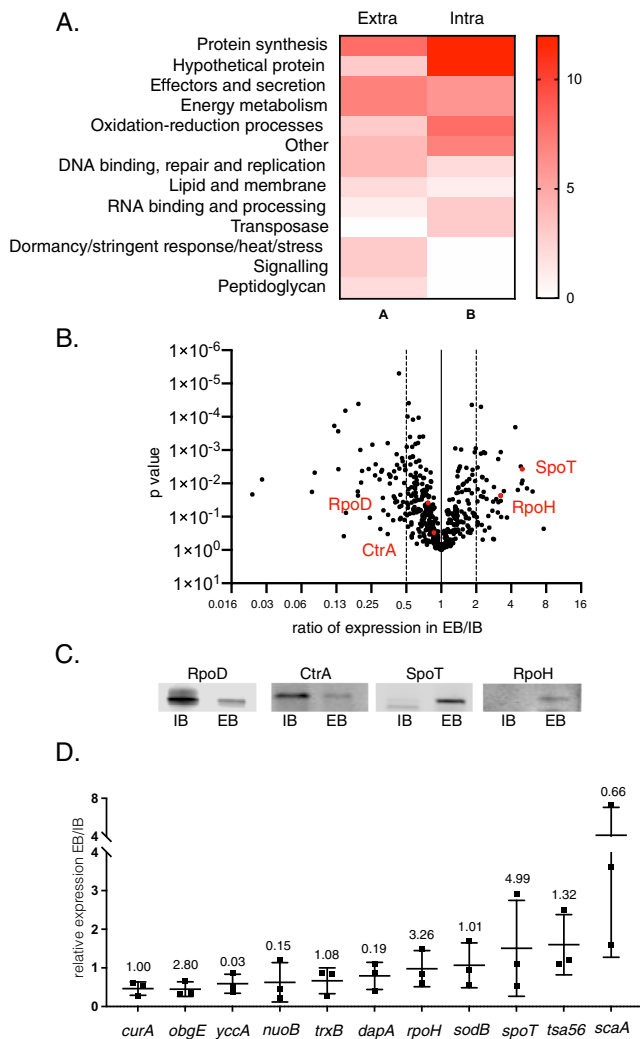
Fig. 3 Intracellular and extracellular forms of Ot have different levels of certain proteins. A Pathway analysis of proteins present at >2X difference between IB and EB forms of Ot (60 proteins in IB, 47 proteins in EB). Bacteria were grown in triplicate in L929 cells at an MOI of 410:1 and harvested 4 days post-infection. IB and EB Ot were isolated and analysed by shotgun proteomics. **B** SpoT and RpoH are present at higher levels in EB compared with IB Ot as measured by proteomics described in **A**. Statistical significance was determined using a *t* test with GraphPad Prism software. **C** Immunoblot analysis showing relative levels of four Ot proteins SpoT, RpoD, RpoH, and CtrA in IB and EB Ot. Loading was normalized by measuring bacterial genome copy number using qPCR and loading the same number of IB and EB Ot in each pairwise comparison. Samples taken from the same experiment are used for the four antibodies in this figure, with the same amount loaded in each immunoblot. Uncropped immunoblot images with molecular weight markers are given in Supplementary Fig. 4. This data confirms the trends observed in the proteomics analysis for these four proteins. **D** RT-qPCR analysis showing relative levels of 11 genes expressed in EB and IB Ot. Bacteria were isolated from L929 cells 4 days post-infection at an MOI of 672:1, 300:1, and 560:1. *n* = 3 independent experiments. Data are presented as mean values ± SD. Gene expression levels were normalized using three genes: *mipZ*, *ank12*, and *16S*. Mean and standard deviation values are shown. The ratio of protein levels in EB/IB, as found in the proteomics experiment in 2A, is given above each gene for comparison.

relative to host cells would exhibit almost identical protein profiles. To test this, we performed shotgun mass spectrometric analyses on isolated IB and EB Ot forms. We found that whilst the correlation coefficient of proteins detected in IB and EB isolated four days post-infection was strong (correlation coefficient = 0.843) (Supplementary Fig. 3) there were several proteins that accumulated to different levels in the two populations. A complete list of the relative levels of proteins detected in IB and EB is provided in Supplementary Data 1. Pathway analyses revealed that IB Ot was enriched in proteins involved in protein synthesis (Fig. 3A). In contrast, EB Ot displayed high expression of SpoT and RpoH, two proteins involved in the stringent response (Fig. 3B). In order to validate these results, we generated antibodies against four proteins that were present at different levels in IB and EB Ot: SpoT, RpoH, RpoD and CtrA. We carried out immunoblot analysis of IB and EB Ot and found that both SpoT and RpoH were present at higher levels in EB than IB, whilst RpoD and CtrA were present at higher levels in IB Ot (Fig. 3C), consistent with the trends observed in our proteomics analysis.

We next investigated whether EB and IB Ot exhibited differences in transcript expression levels. These experiments required the propagation of large amounts of EB because this form of Ot is metabolically inactive and thus harbors very low mRNA levels. We selected 11 genes, three of which (*curA, trxB, sodB*) were expressed at similar levels in our proteomic studies comparing EB and IB. Additionally, we quantified mRNA expression of four genes encoding proteins enriched in IB Ot (*yccA, nuoB, dapA, scaA*) and four genes enriched in EB Ot (*obgE, spoT, tsa56, rpoH*). We isolated RNA from IB and EB bacteria 4 days post-infection and assessed mRNA levels by qRT-PCR (Fig. 3D). Whilst we observed differences in relative mRNA levels between IB and EB for most genes, we frequently found no correlation between mRNA and protein levels for a particular gene. For example, *rpoH* transcript levels were similar in IB and EB Ot, but protein levels were higher in EB. These observations provide additional evidence supporting the existence of molecularly distinct bacterial forms and suggest that transcriptional and post-transcriptional regulatory mechanisms participate in the differentiation process.

Surface proteins are present at different relative levels on IB and EB forms of Ot. Our differential proteomics analyses revealed that IB and EB have different levels of specific surface proteins (Fig. 4A). Surface proteins play a central role in Ot function for two reasons. First, unlike most Gram-negative bacteria, Ot lacks lipopolysaccharide, which generally serves as a membrane shield. Second, Ot is a cytosolic bacterium, and its surface is in direct contact with cytoplasmic host components. Ot harbors genes encoding four widely conserved autotransporter proteins: ScaA, ScaC, ScaD, and ScaE. Using our proteomics dataset, we detected ScaA and ScaC, but not ScaD or ScaE. ScaA was slightly enriched in IB relative to EB Ot (1.5X), while ScaC was enriched in EB (1.87X). Ot also harbors genes encoding three immunogenic surface proteins that dominate the humoral response in human patients, TSA22, TSA47, and TSA56[16]. We found that TSA22 was enriched in IB relative to EB Ot (3.2X) while TSA47 and TSA56 were not present at significantly different levels (1.14X and 1.32X increase in EB compared with IB, respectively). To verify our observations, we generated polyclonal antibodies against ScaA and ScaC and determined their relative levels in IB and EB bacteria using immunoblot analyses (Fig. 4B and Supplementary Fig. 4). Our experiments up to this
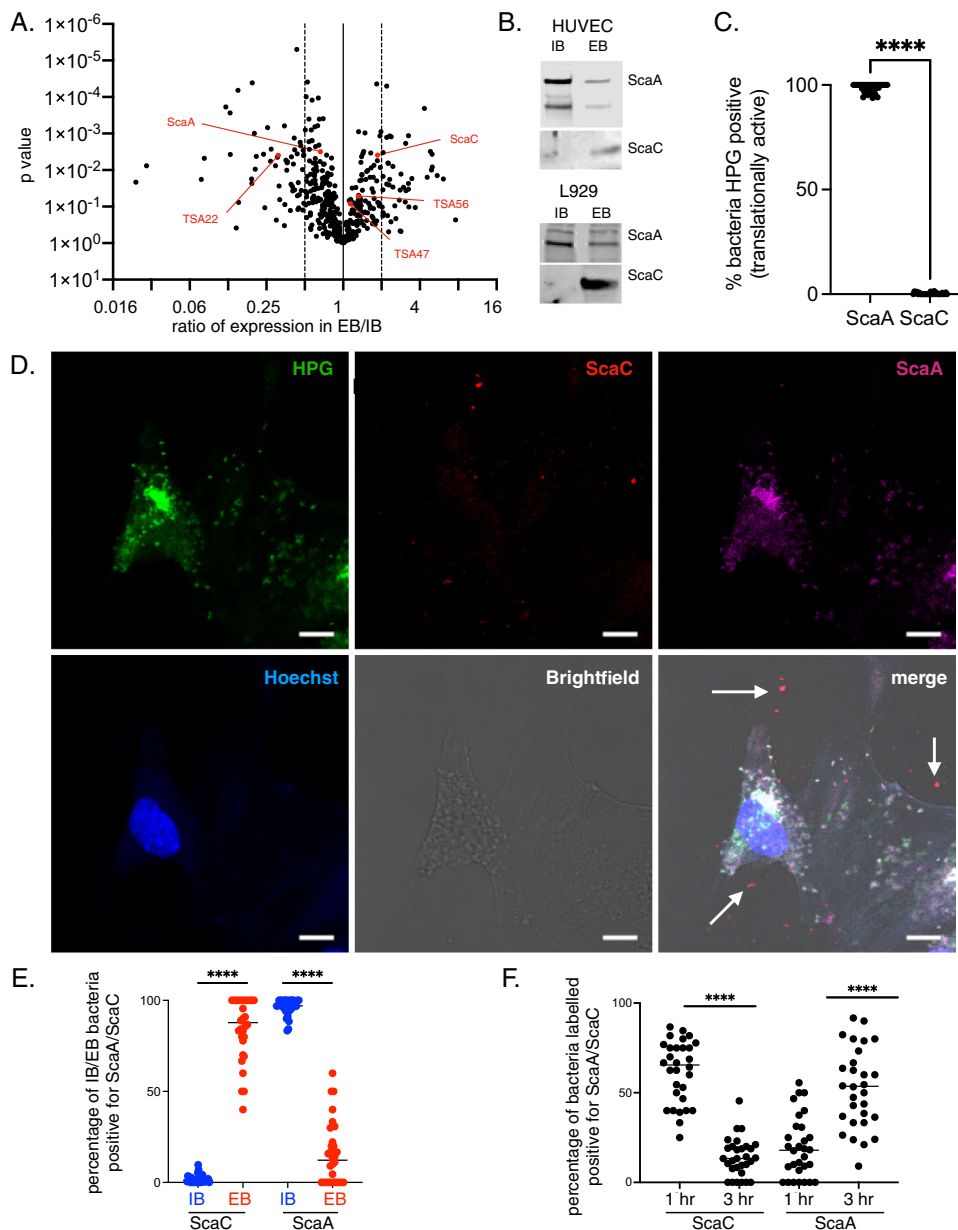
Fig. 4 Autotransporter proteins ScaA and ScaC are differentially expressed on IB and EB forms of Ot. A Volcano plot showing differential expression of surface proteins in proteomics analysis of IB and EB forms of Ot. We observe higher expression of ScaC, TSA56, and TSA47 in EB whilst IB Ot expresses higher ScaA and TSA22 levels. Statistical significance was determined using a t test. **B** Immunoblot analysis of IB and EB Ot from infected L929 and HUVEC cells confirming differential expression of ScaA, and ScaC between IB and EB forms. Loading was normalized by measuring bacterial genome copy number using qPCR. Uncropped immunoblot images with molecular weight markers are given in Supplementary Fig. 4. **C** Quantification of translational activity, as determined by a positive confocal microscopy signal observed with the clickable methionine probe HPG. HUVEC cells were infected with Ot for 5 days, then fixed and labeled with HPG and anti-ScaA/anti-ScaC antibodies. ScaA/ScaC-positive bacteria were scored as being positive or negative for HPG labeling. **D** Confocal micrographs of HUVEC cells infected with Ot for 5 days and labeled for DNA (Hoechst, blue), translational activity (HPG, green), ScaA (anti-ScaA antibody, magenta), and ScaC (anti-ScaC antibody, red). Scale bar = 10 μm. Examples of ScaC-positive extracellular bacteria are shown with a white arrow. More images and equivalent experiments in L929 cells are shown in Supplementary Figs. 5–7. **E** Quantification of experiments described in **D**. The percentage of IB and EB Ot at 5 days post-infection that were positively labeled with anti-ScaA and -ScaC antibodies was counted. **F** Quantification of ScaA- and ScaC-positive IB bacteria inside HUVEC cells one- and three hours post-infection, showing an increase in ScaA labeling and a decrease in ScaC labeling. In (**B**, **E**, **F**). $n = 30$ randomly imaged fields across three independent experiments. Graphs show individual values and means. Statistical significance was calculated using a two-sided unpaired t test with Graphpad Prism software. *p value ≤ 0.05; **p value ≤ 0.01; ***p value ≤ 0.001; ****p value ≤ 0.0001.

point were performed in mouse fibroblasts (L929) because Ot grows readily in these cells. Moreover, L929 fibroblasts are suitable for characterizing bacterial properties that are not affected by the cellular environment. However, for our validation studies, we also investigated bacteria grown in primary human umbilical vein endothelial cells (HUVEC) as a more physiologically relevant model of Ot infection in humans. Our immunoblot studies in both L929 and HUVECs confirmed enrichment of ScaA in IB Ot and higher levels of ScaC in EB compared to IB Ot, in agreement with our mass spectrometric analyses.
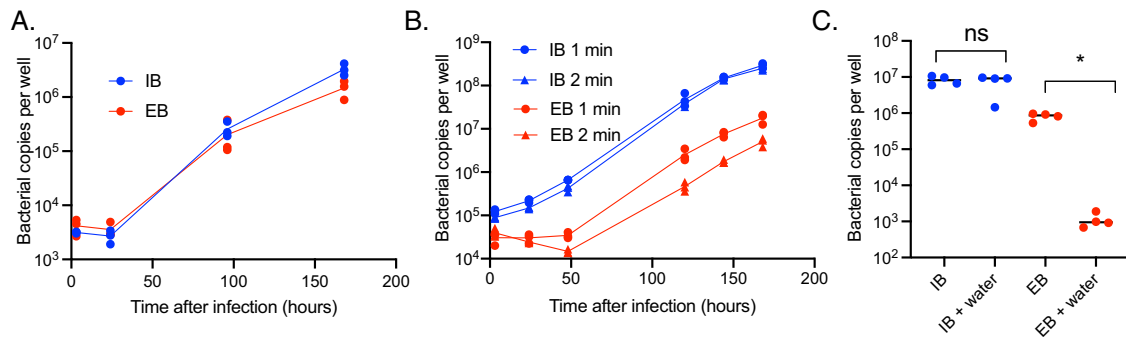
Fig. 5 Both IB and EB populations are infectious but differ in physical stability. IB and EB Ot were isolated from infected L929 cells 5 days post-infection and grown in fresh L929 cells in a 24-well plate. The number of intracellular bacteria was then quantified at 3-, 24-, 96-, and 168 h post-infection using qPCR against *tsa47*, a single copy Ot gene. Doubling times of IB and EB Ot were similar. Similar results were found in HUVEC cells (Supplementary Fig. 8). **B** IB and EB were exposed to physical stress using a bead mill for 1 or 2 min; growth was quantified as in 4A. The bead mill did not affect the growth rate of IB Ot but reduced that of EB Ot in an exposure-dependent manner. **C** IB and EB were exposed to osmotic shock by suspending the bacteria in water for five min and then growing them in fresh L929 cells. Bacterial copy number after 7 days was quantified by qPCR. EB was more susceptible to osmotic shock than IB Ot, as shown by a more significant decrease in bacterial number. Statistical significance was determined using a two-sided Mann–Whitney test. $P = 0.0286$. For (**A**–**C**) each datapoint was taken from a separate well from a 24-well plate.

ScaA and ScaC as preliminary markers of EB and IB forms of Ot. Our observation that 95% of IB is translationally active 5 days post-infection, compared with 0% of EB, combined with the fact that these Ot forms display opposite relative levels of ScaA and ScaC led us to investigate whether these surface proteins can be used as *bonafide* markers of metabolically active IB and metabolically quiescent EB Ot forms, respectively. We used immunofluorescence microscopy to identify bacteria expressing ScaA and ScaC and then quantified the number of translationally active ScaA- and ScaC-positive bacteria by measuring incorporation of HPG. We found (Fig. 4C and Supplementary Fig. 7A) that ScaA-positive bacteria, in contrast to ScaC-positive Ot, were mostly translationally active. We then quantified the number of ScaA/ScaC-positive bacteria inside and outside cells and confirmed that ScaC and ScaA levels were higher in EB and IB Ot, respectively (Fig. 4D, E and Supplementary Figs. 5, 6, 7B). Together, these results show that ScaA and ScaC are present at different relative levels depending on bacterial location relative to host cells: metabolically active IB exhibit higher levels of ScaA relative to EB Ot. Conversely, levels of ScaC in metabolically inactive EB is high relative to that of IB forms of Ot. We therefore propose that ScaA and ScaC can be used as markers to distinguish between IB and EB forms of Ot. However, it is worth noting that the correlation between expression of these proteins and bacterial position relative to host cells is not absolute and it is likely that more robust markers of the different forms of Ot may be uncovered in future studies.

The observation that EB exhibits high *scaA* transcript levels (Fig. 3D) but low levels of ScaA protein led us to hypothesize that ScaA is translated into protein soon after entry into host cells, using pre-formed mRNA. We quantified the number of IB Ot expressing ScaA and ScaC at 1- and 3 h post-infection and found a decrease in ScaC levels and an increase in ScaA levels as the infection proceeded (Fig. 4F and Supplementary Fig. 7C). These results show that ScaA accumulates during the first 3 h after infection, suggesting that *scaA* transcripts are made in EBs in anticipation of new infections. These results point to the existence of regulatory mechanisms that control levels of ScaA and ScaC on the surface of Ot cells, depending on bacterial location and stage of host infection.

IB and EB Ot populations are infectious but differ in physical stability and mechanisms of entry into host cells. Previous studies have shown that certain Anaplasmataceae species differentiate into distinct intracellular and extracellular forms and that only the extracellular form is effective at infecting host cells[17]. This observation led us to investigate whether the ability to infect host cells differs in IB compared with EB Ot. Growth curve measurements revealed that both bacterial forms could infect L929 and HUVEC cells and replicate with similar dynamics (Fig. 5A and Supplementary Fig. 8). However, IB appears to retain infectivity more efficiently than EB following physical and osmotic challenges. Specifically, when we subjected IB and EB Ot to physical stress using a bead mill for 1–2 min, we found that EB displayed a reduction in growth that was dependent on the time of exposure to stress; in contrast, IB was unaffected by this treatment (Fig. 5B). Furthermore, osmotic shock resulted in a significantly greater reduction in viability in EB compared with IB (Fig. 5C). Together, these results demonstrate that IB is physically more robust than EB; this property is likely due to differences in peptidoglycan content, as described above.

To investigate whether EB and IB forms of Ot enter host cells using the same invasion mechanism, we pre-treated HUVEC cells with the clathrin-mediated endocytosis inhibitor dynasore or the macropinocytosis inhibitors amiloride and zoniporide. We then infected the cells with IB or EB Ot and quantified the number of intracellular bacteria 3 h post-infection using confocal microscopy (Fig. 6A, B). The entry of IB Ot into the cells was blocked by dynasore, thus confirming the participation of clathrin-mediated endocytosis in this process. IB entry was also inhibited by amiloride and zoniporide, suggesting additional involvement of macropinocytosis in bacterial uptake. In contrast, EB Ot entry into cells was not affected by dynasore treatment but was completely inhibited by pre-incubation with amiloride or zoniporide. To confirm that EB Ot did not use clathrin-mediated endocytosis to enter cells, we treated HUVEC and L929 cells with siRNA against clathrin. Control microscopy experiments demonstrated that clathrin-targeting siRNA reduced the levels of clathrin foci in uninfected cells (Supplementary Fig. 9). We found that entry of IB form Ot required clathrin, whilst entry of EB form Ot did not (Fig. 6C, D. and Supplementary Fig. 10). Together these results demonstrate that IB form Ot uses clathrin-mediated endocytosis to enter cells whilst EB form Ot does not.

To further demonstrate that IB and EB Ot were entering host cells using distinct mechanisms, we examined the role of the surface adhesins TSA56 and ScaC on bacterial entry. These are
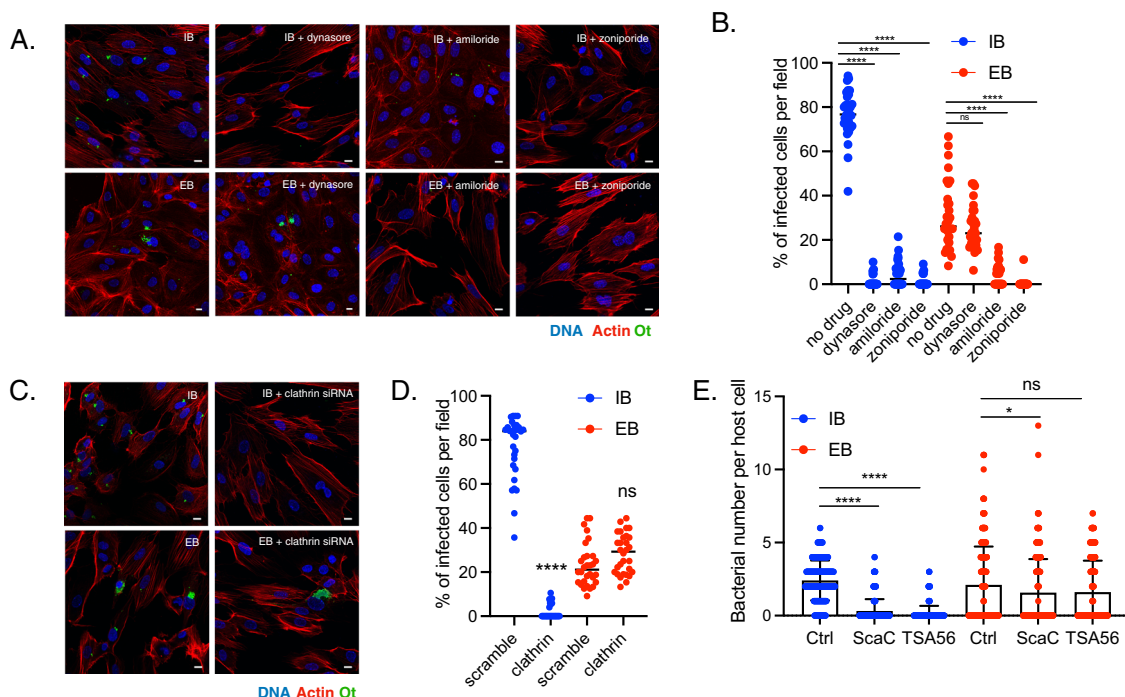
Fig. 6 IB and EB Ot enter host cells using distinct mechanisms. Images (**A**) and quantification (**B**) of the effect of endocytosis inhibitors on entry of IB and EB Ot into HUVEC cells. IB and EB Ot were seeded onto fresh HUVEC cells that had been treated with inhibitors of clathrin-mediated endocytosis (100 μM dynasore) or macropinocytosis (50 μM amiloride or 100 μM zoniporide). Cells were fixed 3 h post-infection. Dynasore inhibits entry of IB but not EB, whilst amiloride and zoniporide inhibited entry of both IB and EB. Red = actin (phalloidin), blue = Hoechst (DNA), green = Ot (anti-TSA56 antibody). Scale bar = 10 μm. Similar results were found in L929 cells (Supplementary Fig. 10). Images (**C**) and quantification (**D**) of the effect of 0.2 μM siRNA against clathrin on entry of EB and IB Ot into HUVEC cells. Experiments were carried out as in **A**, **B**. In **B**, **D**. n = 30 fields randomly imaged over 3 independent experiments. In each field the percentage of infected host cells was counted. Individual values and means are shown here. Statistical significance in **B** was determined by comparing all groups using one-way ANOVA, followed by a Dunnett's multiple comparison tests with the control within the IB or EB group, and in **D** by performing a Mann–Whitney test comparing the scramble control and the clathrin siRNA treated condition for IB and EB separately. **E** Blocking the bacterial surface adhesins TSA56 and ScaC with anti-TSA56 and anti-ScaC antibodies strongly inhibits entry of IB but not EB Ot in HUVEC cells. Bacterial entry in the presence of vehicle control or antibodies was determined by quantifying the number of intracellular bacteria per host cell 30 min post-infection using immunofluorescence microscopy of bacteria labeled with HPG. Statistical significance was determined by comparing all groups using one-way ANOVA, followed by a Dunnett's multiple comparison tests with the control within the IB or EB group. ****p ≤ 0.0001; ns not significant. *p value ≤ 0.05; **p value ≤ 0.01; ***p value ≤ 0.001; ****p value ≤ 0.0001.

outer membrane proteins that have been shown to be involved in entry of Ot into host cells, in experiments carried out using what we now describe as IB Ot stage bacteria[6,7]. We used antibodies targeting ScaC and TSA56 and determined whether these antibodies would block the entry of Ot into host cells. Our results with IB Ot replicated published studies and showed that blocking ScaC and TSA56 using antibodies led to a strong reduction in bacterial entry (Fig. 6E). With EB Ot, however, only a minimal effect was observed (Fig. 6E). This result is consistent with a model in which IB Ot enters host cells using adhesin-induced clathrin-mediated endocytosis, whilst in EB Ot the surface proteins are shielded by host derived membrane and the bacterium enters cells through macropinocytosis.

Discussion

Our studies have unveiled a new feature of the obligate intracellular bacterium Ot. This organism's unique exit strategy, which involves budding off the surface of infected cells, is associated with differentiation into a molecularly and functionally distinct developmental state (Fig. 7). While unusual in the family Rickettsiaceae, this property is reminiscent of the biphasic lifecycle of multiple species in the sister family Anaplasmataceae[4] and the unrelated obligate intracellular bacteria Chlamydia spp[18]. However, in contrast to these organisms,

Ot resides in the host cytosol in naked form rather than in a membrane-bound vacuole. To our knowledge, this is the first description of an intracellular bacterium living freely in the host's cytosol and having a biphasic lifecycle. Our findings have important implications for our understanding of Ot biology and unveil opportunities to develop better therapeutic strategies to treat scrub typhus.

The physical properties of prokaryotic cell walls are crucial for survival. These stiff structures maintain cellular shape, protect the interior, counteract osmotic pressure, and provide structural strength through peptidoglycan layers. Our studies revealed that EB and IB forms of Ot differ in peptidoglycan content. Lower levels in EB compared with IB make this form more susceptible to physical and osmotic stress. There is a long-standing question regarding the role of peptidoglycan in obligate intracellular bacteria. These organisms reside in an osmotically protective niche and are under selective pressure to reduce the abundance of immunogenic pathogen-associated molecular patterns (PAMP)s[19]. In the case of pathogenic Chlamydia species, it has been shown that peptidoglycan is retained only at the septum and is required for cell division[20]. Higher peptidoglycan levels in IB Ot vs. EB Ot point to the retention of a peptidoglycan-like structure for growth and division rather than structural integrity maintenance.
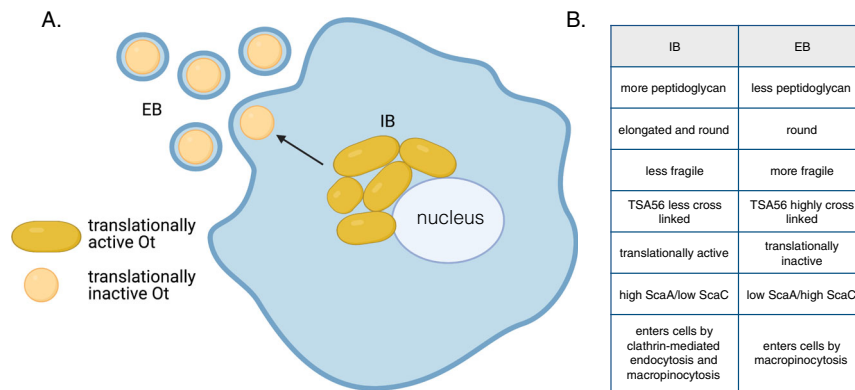
Fig. 7 An overview of the infection cycle of Ot, showing differentiation between IB and EB forms. A IB replicate in a micro-colony adjacent to the nucleus where they are elongated in shape and translationally active. Bacteria move to the cell's edge and transition to an EB form that is round and translationally inactive. Created with BioRender.com. **B** Table summarizing the differences between IB and EB forms of Ot.

The observed differences in physical properties between EB and IB forms are complemented by measurable differences in the accumulation of certain proteins, suggesting that each form performs unique functions or responds to specific challenges. Proteomics analyses in EB Ot revealed increased levels of heat shock sigma factor RpoH and the alarmone (p)ppGpp synthetase SpoT associated with the stringent response[21]. These results suggest that the EB form of Ot shares features with the dormant state of other bacteria. Notably, Ot is the only reported member of the Rickettsiaceae to encode a full-length *spoT* gene[4]. This exclusive feature is consistent with the fact that developmental differentiation of Ot is highly unusual in members of this family. The changes associated with differentiation into the EB state likely serve one or both of the following purposes: ensuring survival in the extracellular state and priming the bacteria for reinfection of new cells. Indeed, the observation that *scaA* transcripts are abundant in the EB form and that ScaA protein is synthesized early upon entry into host cells supports the idea that EB Ot is primed for infection.

Comparing the protein and RNA transcript levels of selected genes revealed a poor correlation for many genes. A potential explanation is that RNA levels are low in the metabolically inert EB form, which does not reflect newly translated proteins. Ot strain UT76 encodes only 8 predicted transcription factors and two sigma factors, RpoD and RpoH[22]. Thus, it is possible that gene expression is not strictly regulated at the transcriptional level but that other forms of regulation are prevalent in Ot. We recently showed high antisense transcription levels in Ot, especially in genes associated with the rampant integrative conjugative element RAGE, which dominates the Ot genome[23]. There, we found that high antisense transcription correlates with low protein levels for a particular gene, pointing to this mechanism as a central regulatory strategy in Ot. Gene expression in the Ot-related, free-living alphaproteobacterium *Caulobacter crescentus* is highly regulated by proteolysis[24]. Mechanisms based on differential proteolysis may therefore also play an essential role as critical determinants of protein levels in Ot.

Our observation that EB Ot enters cells through macropinocytosis, whereas IB Ot utilizes endocytosis and, to a lesser extent, macropinocytosis resolves a long-standing gap in the field as it was unclear how budded bacteria enveloped in plasma membrane enter host cells. Physiologically, IB entry into host cells may be necessary during trafficking into adjacent cells, as previously described for spotted fever group *Rickettsia* spp.[25]. Additionally, low levels of cell lysis may release IB Ot forms that

can then infect new host cells. The different mechanisms utilized by EB and IB to enter cells suggest that strategies to escape from the endolysosomal pathway will differ between the two Ot forms. It is unclear whether and how the differing transcriptional and proteomic profiles at the point of infection will affect early host-pathogen interactions. Our finding that IB and EB's growth dynamics are similar suggests that early differences do not persist through the infection cycle.

In summary, our finding that Ot differentiates into molecularly and functionally distinct forms provides a novel framework to study the infection cycle of this important obligate intracellular pathogen and opens avenues to investigate the physiological significance of the distinct populations characterized.

Methods

Cell culture, bacterial propagation and quantification, and reagents. Proteomics and qRT-PCR experiments were performed using the mouse fibroblast cell line L929 kindly provided by Dr. Blacksell at the Mahidol Oxford Tropical Medicine Research Unit, Bangkok, Thailand. For all other experiments, we used L929 cells (ATCC CCL-1), Primary Human Umbilical Vein Endothelial Cells (HUVEC) (ATCC PCS-100-010) or monkey kidney epithelial Vero cells (ATCC CRL-1586) all purchased from ATCC. We cultured cells in either DMEM (L929) or Large Vessel Endothelial Supplement (LVES, HUVEC) supplemented with 10% FBS (Gibco 16140071) at 37 °C and a 5% CO_2 atmosphere. The Karp-like clinical isolate strain of Ot UT76[22] was used throughout the study. For routine propagation, bacteria were grown in 25- or 75-cm^2 culture flasks, as described previously[12]. We extracted DNA using alkaline lysis buffer[12], and then assessed bacterial quantities by determining genome copy numbers relative to a standard curve, using Biorad CFX Maestro manager software v3.1. We used a primer/probe set to amplify the single copy gene *tsa47* (tsa47F 5′-TCCAGAATTAAATGAGAATTTAGGAC-3′, tsa47R 5′-TTAGTAATTACATCTCCAGGAGCAA-3′, tsa47probe 5′-[6FAM] TTCCACATTGTGCTGCAGATCCTTC[TAM]-3′) or the 16S gene (Rick16SF 5′-GCTACACGCGTGCTACAATGG-3′, Rick16SR 5′-TGTGTACAAGGCCCGAG AACG-3′, Rick16Sprobe 5′-[6FAM] ATCGCTAGTAATCGCGGATCAGCA TGCC [TAM]-3′). For drug inhibition assays, dynasore (Sigma D7693) and amiloride (Sigma A3085) were added to L929 or HUVEC cells 1 h before infection with Ot.

Fluorescence microscopy

Immunofluorescence labeling and confocal microscopy. Following fixation, cells were permeabilized by incubation in 0.5% Triton X-100 for 30 min on ice followed by blocking in 1XPBS (pH7.4) containing either 1 mg/ml BSA or sera (diluted 1:20) matching the labeled antibody's host, for 30 min at room temperature. Incubations with primary antibodies took place for 1 h at 37 °C. These studies were conducted using in-house-generated antibodies (i.e., rat monoclonal antibody against TSA56 diluted 1:200; rabbit polyclonal antibody against Ot ScaC diluted 1:200) or commercial products (i.e., MA1-065, a ThermoScientific monoclonal mouse antibody against clathrin heavy chain diluted 1:200). The fixed cells were washed twice with PBS-BSA and were then incubated with appropriate secondary antibodies (1:1000 dilutions) for 30 min at 37 °C in the dark. We used the following secondary antibodies: goat anti-mouse IgG superclonal Alexa Fluor 647 conjugate (ThermoFisher A28180), goat anti-rat Alexa Fluor 488 (ThermoFisher A11006), and

goat anti-rabbit Alexa Fluor 594 (ThermoFisher A11012). The nuclear stain Hoechst (1:1000 dilution) was supplemented to incubations with secondary antibodies. Phalloidin Alexa Fluor 594 (1:200, ThermoFisher Scientific A12381) was used to detect host actin. The cells were washed with 3X PBS before supplementation of mounting medium [20 mM Tris (pH 8.0); 0.5% N-propyl-gallate; 90% glycerol]. Imaging was performed using a Zeiss Observer Z1 LSM700 confocal microscope with an HBO 100 illuminating system equipped with a 63×/1.4 Plan-APOCHROMAT objective lens (Carl Zeiss, Germany) and 405 nm, 488 nm, and 555 nm laser lines or a Leica TCS SP8 confocal microscope (Leica Microsystems, Germany) equipped with a 63×/1.4 Plan-APOCHROMAT oil objective lens with a 1.4-mm working distance and 405 nm, 488, 552, and 638 nm laser lines acquired using Leica TCS SP8 software.

Fluorescence intensity measurements were performed manually using Fiji Image J software. 30 (Fig. 4C) or 100 (Fig. 2B); individual bacteria were quantified by measuring the brightest pixel intensity within the bacterial area. Images from individual experiments were acquired under identical laser intensity and acquisition conditions. Length and width measurements were performed manually using Fiji Image J software.

STORM imaging and analysis. We acquired 3D-STORM data using a homebuilt multi-color Total Internal Reflection Fluorescence (TIRF) microscope[26] that is based on an inverted microscope (Nikon, Ti-E), a high NA objective (Nikon, CFI-Apo 100X, NA 1.49), a 405 nm photoactivation laser (Coherent, OBIS 405 LX 100 mW), a 488 nm excitation laser (MPB, 2RU-VFL-P-20000642-B1R), and an EMCCD camera (Andor, iXon Ultra-888). Samples immunolabelled with Alexa 488 were mounted on the microscope, transferred to STORM buffer [OxyFluor (Oxyrase), 50 mM betamercaptoethanol (Sigma), 2.5 mM cyclooctatetraene (COT) (Sigma)], and illuminated with a strong (488 nm) laser to record single-molecule fluorescence blinking events at a frame rate of 25 Hz. Illumination at 405 nm was intercalated with pulsed 488 nm excitation to enhance photoactivation of Alexa 488 without exacerbating background signal. A cylindrical lens (Thorlabs, LJ1516RM-A) was placed in front of the camera to determine the z-coordinates of fluorescent molecules through the elongated point spread function (PSF) methods[27]. Each STORM image was reconstructed from single-molecule localization data obtained by analysing 30,000 frames with custom Matlab codes. Briefly, bright single fluorescence spots were identified by thresholding methods, and their 3-D coordinates were determined by 2-D elliptical Gaussian fitting along with a pre-calibrated conversion table between eccentricity and z-coordinate. Focus drift was actively stabilized with Perfect Focus System (Nikon) while acquiring the data, whereas xy-drift was post-corrected using a redundant cross-correlation algorithm[28]. Each localization event was represented as a 2-D Gaussian of 20 nm standard deviation in STORM images. For the analysis of bacterial morphology, we selected cells that showed clear cell boundary, manually adjusted the z-coordinate to locate the cell mid-plane and measured long- and short-axes length.

Click labeling. Our metabolic click labeling was based on the Click-iT HPG Alexa Fluor protein Synthesis Assay Kit (Click-iT HPG Alexa Fluor Protein Synthesis Assay Kit, ThermoFisher C10428) strategy. To incorporate L-homopropargylglycine (HPG), we incubated infected cells with minimal medium (Dulbecco's Modified Eagle Medium, DMEM, ThermoFisher 21013) lacking L-methionine and containing 25 μM HPG, for 30 min at 37 °C. Labeled bacteria were washed twice with PBS containing 1 mg/ml BSA, fixed with 1% formaldehyde, and subsequently permeabilized with 0.5% Triton X-100 for 20 min on ice. After further washing with PBS containing 1 mg/ml BSA, we supplemented the Click-iT reaction cocktail (Click-iT HPG Alexa Fluor Protein Synthesis Assay Kit, ThermoFisher C10428) and incubated the cells for 30 min at room temperature in a light protected environment. The Azide dye (Alexa Fluor 488) was used at a final concentration of 5 μM. Following completion of the click reaction, the cells were subjected to immunofluorescence labeling and imaging as above.

Gene expression analysis by RT-qPCR. L929 cells were infected with Ot using multiple MOIs to a target MOI of 400:1 (quantitative PCR on freshly isolated Ot showed variation of actual MOIs ranging from 200:1 to 672:1 across three independent infections). Very high MOIs were used due to the low levels of EB bacteria combined with the fact that RNA levels in EB Ot were very low. Infected cells were harvested 4 days post-infection and were stored in RNAProtect Bacteria Reagent (Qiagen 76506) at −80 °C. Total RNA was extracted using the Qiagen RNeasy Plus kit (Qiagen 74136) according to the manufacturer's instructions. One μg of total RNA was incubated with DNaseI (ThermoFisher Scientific, AM2238) for 16 h at 37 °C, and the samples were then reverse-transcribed using the iScript reverse transcription supermix (Biorad 170−8841) and random primers. Controls lacking reverse transcriptase demonstrated that the RNA sample used for cDNA synthesis was not contaminated with genomic DNA. The resulting cDNA was then used as template for qPCR using primers for *spoT, rpoH, obgE, yccA, nuoB, dapA, curA, sodB, trxB, tsa56,* and *scaA.* RT-qPCR was performed using SYBR green qPCR mix (Biotools 10.609). Expression levels were normalized relative to an average of three genes:*16sRNA, ank12_1,* and *mipZ.*

Primer name	Primer sequences (5′ to 3′)
spoT forward	GGCAGACATAAAGCACCTTAC
spoT reverse	GAAATCTTGAAAGCTGCCAGG
rpoH forward	CTGCCGAAGAGGAATATATGC
rpoH reverse	CCCCTCGGAAACTAAATCAAC
obgE forward	GCACAAAATGGTAGAGCTGG
obgE reverse	GAATCACCAATCTCACCTACAG
yccA forward	GCTATTGCAGGAACCGCTAC
yccA reverse	CTGAAAGCGACATGCCTACA
nuoB forward	GGGCTAGAACACGCTCGTTA
nuoB reverse	GCACAGCTACCCATTGATATC
dapA forward	GGTAGAACATTAGTGATTGCTGG
dapA reverse	GCGTCTTTGATTGCTACTATCC
curA forward	AGTAGGGCAACGAGTTGGC
curA reverse	CAACAGCGCTACTAGCAGC
sodB forward	GTAGTGGTTGGGTCTGGTTG
sodB reverse	GTTCAGCAAATCGCCAATTTG
trxB forward	GATATGCACTGGTGCTCAAG
trxB reverse	CACCTCCTACAACAACTACTC
tsa56 forward	TGCCCAACAAGAAGAAGATG
tsa56 reverse	TTTAACTTGGCCGACAATCA
scaA forward	TAGTGAAAGGGGACGATTGC
scaA reverse	ATCCGACAAGTTAGGCATGG
16sRNA forward	CGGTGAATACGTTCTCGGG
16sRNA reverse	GAGGTAATCCAGCCGCAGG
ank12_1 forward	GATAGCAGAGGTTGTACACCG
ank12_1 reverse	CTGATTTGTTAGGCTGCCTGC
mipZ forward	GTGGTGCAGGTAAGACTACTGTTG
mipZ reverse	GTGAATGCTGACGTGAATCAG

Proteomics sample preparation. We used Ot to infect L929 mouse fibroblasts at a 410:1 MOI in six independent culture flasks. High MOIs were used to ensure sufficient material for proteomics analysis. Despite the high MOI the L929 cells remained intact and attached to the surface of the flask at the point of harvesting the samples. We replaced the culture medium at 1-day post-infection (dpi) to remove bacteria that failed to enter the host. Intracellular and extracellular bacteria were isolated at four dpi; two separate flasks were harvested as one replicate, yielding a total of three replicates. L929 cells were grown in 75-cm² plastic flasks at 37 °C in a 5% CO₂ atmosphere, using DMEM media (Gibco 11965092) supplemented with 10% FBS (Sigma-Aldrich F7524). At four dpi, the media were transferred to 50-ml conical tubes for extracellular bacteria isolation. Culture flasks were rinsed with 15 ml of PBS, and cells were scraped using 2 ml of fresh media per flask. The detached cells were transferred to 2 ml Safe-lock tubes (Eppendorf 0030120094) and homogenized for 3 min using a Bullet blender® homogenizer (Next Advance #BBY24M) with speed control setting at 8. Host cell debris was removed by centrifugation at $300 \times g$ for 3 min; we then harvested intracellular bacteria (IB) by an additional 3 min centrifugation at $20,000 \times g$. Before isolation of extracellular bacteria (EB), we removed possible detached host cells containing IB through a pre-spin step ($1000 \times g$, 5 min, 4 °C). No visible pellet was observed indicating that there were negligible amounts of detached host cells potentially contaminating the EB prep with IB bacteria. Following transfer of supernatants to new conical tubes, we harvested extracellular bacteria by centrifugation at $3000 \times g$ for 20 min at 4 °C. IBs and EBs were washed with 0.3 M sucrose three times, resuspended in PBS, and lysed with 1% Triton X-100 for 30 min at 4 °C. Bacterial proteins were precipitated by addition of 80% ice-cold acetone and overnight incubation at −20 °C. Protein pellets were washed in acetone twice to remove residual Triton X-100 by centrifugation at $15,000 \times g$ for 10 min. Briefly dried protein extracts were then dissolved in 100 μl of 50% trifluoroethanol in 100 mM Triethylammonium bicarbonate (TEAB) buffer. The samples were reduced by treatment with 20 mM tris(2-carboxyethyl)phosphine (TCEP) for 20 min at 55 °C, alkylated in 55 mM chloroacetamide (CAA) at room temperature in the dark, and digested with endoproteinase LysC (LysC: protein ratio = 1:50) overnight at 37 °C and, subsequently, with trypsin (trypsin: protein ratio = 1:100), also overnight at 37 °C. Average bacterial copy numbers for IBs and EBs were estimated by quantitative PCR yielding 1.5E + 08 and 2.6E + 09 per replicate, respectively. The whole protein content in each replicate was used without normalization at this step due to the fact that IBs and EBs were isolated from different environment and therefore have diverse amounts of co-purified host protein. Samples were acidified with Trifluoroacetic acid (TFA) to 1% final concentration and centrifuged to remove insoluble materials. Trypsinized samples were desalted using an Oasis® HLB 1cc cartridge (Waters™). Briefly, following cartridge activation with 500 μl of 100% acetonitrile and equilibration with 500 μl of 0.5% acetic acid, we loaded samples and then washed the cartridge with 1 ml MS-grade water. Peptides were eluted with 500 μl of 80% acetonitrile in 0.5% acetic acid, then transferred to low-binding microtubes, and dried using a SpeedVac. Each peptide pellet was resuspended with 20 μl of MS-grade water. We estimated peptide content using 5% of each sample, so called "Mini-runs". This was to check whether we need to adjust or normalize sample loadings in the actual runs. Briefly, individual aliquots in 1 μl of peptides

were supplemented with 4 μl of 1% (v/v) acetonitrile containing 0.06% (v/v) tri-fluoroacetic acid and 0.5% (v/v) acetic acid, transferred to a 96-well autosampler plate, and then injected (3 μl) into an Orbitrap Fusion™ Mass Spectrometer. After we screened out host proteins from the Mini-runs result, the frequency distribution of Ot protein abundances were plotted. Medians of IB and EB replicates showed abundance values with maximum difference of 1 log scale, suggesting a single normalization process may be performed during data analysis. We decided to fractionate the rest of samples without the need of normalizing sample loadings. The remaining 95% of each sample (19 μl in MS-grade water) was mixed with 20 μl of 10 mM ammonium formate (pH 10) and centrifuged at $20,000 \times g$ for 3 min to eliminate insoluble components. Each peptide sample was then fractionated through a step-wise desalting process on C18 stage tips using 10, 15, 25, and 50% acetonitrile in 10 mM ammonium formate (pH 10). Fractionated samples were washed with 60% acetonitrile containing 0.1% formic acid twice to eliminate residual ammonium formate by evaporation before tandem MS analysis.

LC-MS/MS. Dried samples were resuspended in 10 μl of 2% (v/v) acetonitrile containing 0.06% (v/v) trifluoroacetic acid and 0.5% (v/v) acetic acid, and 1 μl was loaded onto an autosampler plate. Online chromatography was performed in an EASY-nLC 1000 (ThermoScientific) instrument using a one-column setup and 0.1% formic acid in water/0.1% formic acid in acetonitrile as mobile phases. The samples were injected and separated on a reversed-phase C18 analytical column (EASY-Spray LC Column, 75 μm inner diameter × 50 cm, 2 μm particle size; ThermoScientific) maintained at 50 °C and using a 2–23% (v/v) acetonitrile gradient over 60 min, followed by an increase to 50% over the next 20 min, and to 90% over 5 min. The final mixture was maintained on the column for 5 min to elute all remaining peptides. Total run duration for each sample was 90 min at a constant flow rate of 300 nl/min.

Data were acquired using an Orbitrap Fusion Lumos™ mass spectrometer (ThermoScientific) using the instrument's data-dependent mode and using Orbitrap Fusion Lumos Tune Application (v3.3.2782.23). Samples were ionized using 2.5 kV and 300 °C at the nanospray source; positively-charged precursor MS1 signals were detected using an Orbitrap analyser set to 60,000 resolution, automatic gain control (AGC) target of 400,000 ions, and maximum injection time (IT) of 50 ms. Precursors with charges 2–7 and having the highest ion counts in each MS1 scan were further fragmented using collision-induced dissociation (CID) at 35% normalized collision energy. MS2 signals were analysed by ion trap at an AGC of 15,000 and maximum IT of 50 ms. Precursors used for MS2 scans were excluded for 90 s to avoid re-sampling of high abundance peptides. The MS1–MS2 cycles were repeated every 3 s until completion of the run.

Proteomic data analysis. Proteins were identified using Proteome Discoverer™ (v2.3, ThermoScientific). Raw mass spectra were searched against Ot primary protein sequences derived from complete genome data for the UT76 strain. Mouse whole proteome sequences were obtained from Uniprot and included as background. Carbamidomethylation on Cys was set as a fixed modification; deamidation of asparagine and glutamine, acetylation on protein N termini, and methionine oxidation were set as dynamic modifications for the search. Trypsin/P was set as the digestion enzyme and was allowed up to three missed cleavage sites. Precursors and fragments were accepted if they had a mass error within 10 ppm and 0.8 Da, respectively. Peptides were matched to spectra at a false discovery rate (FDR) of 1% against the decoy database.

For label-free quantitation (LFQ), features were extracted from the raw data files using the Minora Feature Detector processing workflow node on Proteome Discoverer. Chromatographic feature-matching was performed with a tolerance of 10 min to align the retention times and enable quantitation of the precursors. No pre-normalization was performed using the Proteome Discoverer workflow, and raw results were manually normalized using the Median normalization method. A protein was classified as detected if at least two peptides were detected in a minimum of two biological replicates; the mean LFQ across the three replicates was used for further analyses. There was no normalization during protein treatments and peptide injection as described earlier. Normalization between samples was performed only in the data analysis process. Briefly, frequency distributions of Ot protein abundances from six separate runs were plotted (excluded co-purified host proteins). And the median from each plot was used to normalize the whole set, prior to data trimming, making all dataset scaled to the same median reference value of 1. Normalized abundance values were then averaged from independent biological replicates (Supplementary Data 1). Statistical significance (t test) was calculated using GraphPad Prism software 8.4.3. Subsequently, proteins detected in both IBs and EBs for at least twice were selected for protein abundance comparison, described as Ext/Int ratio. Proteomic data is available from the jPOST repository with the identifier PXD028218.

Immunoblot analyses. L929 and HUVEC cells were grown in 24-well plates and infected with Ot at an MOI of 12:1. Noninfectious bacteria were removed by replacing the media 24 h post-infection. EB and IB populations were prepared 4 days post-infection. EB was prepared by transferring the cell supernatant to an Eppendorf tube, pelleting at $16,873 \times g$, then resuspending in 100 μl PBS containing 1× protease inhibitor cocktail (ThermoFisher 78425). For TSA56 immunoblots, samples were prepared in the presence of 1 mM iodoacetamide (Sigma-Aldrich catalog number I6125). IB was prepared by removing adherent cells using trypsinization, spinning the cell pellet, and resuspending it in PBS supplemented with protease inhibitors; host cells were lysed using a bead mill for 1 min. Host cell debris was removed by centrifugation at $500 \times g$ for 5 min; the supernatant was transferred to a clean tube, spun at $16,873 \times g$ for 5 min, and resuspended in 100 μl PBS supplemented with protease inhibitors. Bacterial copy number was quantified by qPCR using *tsa47* primers, as described above. IB and EB samples were diluted to ensure equal loading of bacterial cells on gels. Samples were diluted in 5X SDS loading buffer with and without ß-mercaptoethanol and heated at 95 °C for 5 min. Samples were subjected to electrophoresis on a 4–20% gradient gel (BioRad 4561094) and then transferred to a nitrocellulose membrane. Following blocking in PBST containing 5% BSA and 5% skim milk for 30 min, we incubated the blots with primary antibody (1:1,000) in PBST-BSA overnight at 4 °C. Membranes were washed and incubated with secondary antibody (1:10,000) conjugated to IRDYE 680RD or IRDYE 800CW (LI-COR Biosciences) in PBST-BSA for 1 h at room temperature. Membranes were washed, and immunoreactive proteins were visualized using a LiCor Odyssey CLX imager and analyzed using Image Studio V3.1.

Quantification of genome copy number per cell. The genome copy number per cell was calculated by determining the number of bacterial genome copies in a sample of purified EB and IB Ot, using *tsa47* qPCR, and dividing by the number of bacterial cells in the same sample, as measured by confocal microscopy. Three μl of purified bacteria were spread evenly across a well of a multi-well slide, dried, and

Antibody name	Epitope used for immunization	Description of epitope	Species and type
TSA56	KLTPPQPTIMPISIADRDF- KLH	Synthetic peptide from strain Karp conjugated to KLH carrier protein	Rat monoclonal
RpoD	MASLRNKNNKIIICNKKTKKNTNVEELASNFVDESEKLSSKISDSDIN LDKDFDYTKLGVCPDKIEEEVALASNATEGEFEEDLDDNIYSTDIVRAYLKDMSN	Recombinant protein M1-N103 from strain Karp	Rabbit polyclonal
CtrA	KGHSEAVIRVGHLSINLDTRSVSMYNKDKQKNMPIHLTNKEYKILE LLAIKKGTVLTKEMFLSHLYSGIDEPEIKIIDVFICKLRRKLEKASNGINFI ETVWGRGYIFAEFKSNDNNYSLNNVEEE	Recombinant protein K120-E145 from strain Karp	Rabbit polyclonal
SpoT	ELSPIAISDNNKIDKINQNLPIDFAKCCYPLPGDLIIGLCTKTEIVIHTTYCTIASN YVLESIRLLDFSWTSNAQKMFYTSSVQLSVRNKIGSLASITTILENNNV	Recombinant protein E556-V661 from strain Karp	Rabbit polyclonal
RpoH	NSSDYKQIADESGVSIAEVSEVNQRLSNSDLSLNTPISYHEDDATELVELVPEHRPNQ EIILANQQDLNLKKEVLQNALQTLTQRELYIIRARKLQDEPDTLEKLSLHFNVSKE RIRQIESKAFEKLQQYVMNTKHKLLHFV	Recombinant protein N158-V299 from strain Karp	Rabbit polyclonal
ScaC	KLH-KIQLQQLQVTLQNSLFLQNKNNNPA + KLH-IAEVSKLLCMLE	Synthetic peptides from strain Karp conjugated to KLH carrier protein	Rabbit polyclonal
ScaA	NNTTESSNDNQGDTGSGATSNPSNPSNPIEGASGTSPATGASDTTGDS DAAGNKEAAGDDSVTDSGASQSNNTTESSNDNQGDTGSGATSNPSNPIE GASGTSPATGASDATGVTETTGGSATGGEVTDG	Recombinant protein N50-G179 from strain Gilliam	Rabbit polyclonal

labeled for immunofluorescence microscopy using TSA56, as described above. The bacteria in a selected field were manually counted to determine the number of bacterial cells in the sample.

Quantification of relative peptidoglycan levels using NOD1 reporter assay. HEK-Blue hNOD1 cells (Invitrogen, hkb-hnod1, USA) were grown in DMEM containing 4.5 g/l glucose, 10% heat-inactivated FBS, 100 U/ml penicillin, 100 mg/ml streptomycin, 100 mg/ml Normocin, 2 mM L-glutamine, and the selective antibiotics blasticidin (30 μg/ml) and Zeocin (100 μg/ml). The cells were seeded on clear-bottom black 96-well plates (Corning 29444-008) 2 days before treatment. Bacterial aliquots from stocks kept in sucrose phosphate glutamine (SPG) at −80 °C were heat-inactivated at 90 °C for 30 min before supplementation to host cells. These studies were carried out in triplicate. After 2 days, growth media were replaced with HEK-blue detection media (Invivogen hb-det2) for SEAP assessment. The plates were further incubated for 6 h at 37 °C in a 5% CO_2 atmosphere and then analyzed spectrophotometrically (Synergy H1, Biotek) at 640 nm. Results were analyzed by GraphPad Prism (GraphPad Software, San Diego California USA), and a t test was performed to compare bacterial SEAP levels to positive control iE-DAP (γ-D-Glu-mDAP) at 10 μg/ml.

Growth curve measurements and bead mill treatment. To determine the growth rate of IB and EB Ot from frozen stock were first grown in two T25 flasks containing a monolayer of L929 cells. At 6 days post-infection, IB and EB were prepared and used to inoculate fresh L929 cells and the subsequent bacterial growth was measured. *EB isolation*—the supernatant portion of the culture consisting of EB was transferred to a 50-mL centrifuge tube (Corning 430828) and subjected to a first centrifugation to remove any host cells at $1500 \times g$ for 5 min. The supernatant was then transferred into a new 50-ml tube and centrifuged at $3220 \times g$ for 20 min to obtain an EB pellet which was resuspended in the fresh media and ready for the next step. *IB isolation*—fresh media was added directly to the culture flasks containing infected cells and these were disassociated from the adherent surface by using a cell scraper (Corning Falcon, catalog no. 353089). The infected cell suspension was then pipetted into a sterile 2-mL microcentrifuge tube. (Eppendorf 022363352) pre-filled with sterile 0.1–0.15 mm diameter glass beads (Biospec 11079101) before introduced to VWR® Bead Mill Homogenizer (VWR 10158-558) at speed 5 for 1 min to break the host cells. Subsequently, the purified IB in the supernatant was separated from host cells debris and glass beads by transferring the supernatant into a new 2-mL microcentrifuge tube and spinning at $300 \times g$ for 5 min. The bacterial concentration in both EB and IB suspension was quantified by qPCR as described above, and EB and IB Ot was infected onto a fresh monolayer of L929 cells in 12-well plates (ThermoScientific 150628). Bacteria were added at $2.83E + 04$ bacterial copies/well which corresponds to an MOI of ~1:10. The number of intracellular bacteria was then measured at 3, 24, 96, and 168 h post-infection by *tsa47* qPCR. *Physical stress induced by bead mill*—IB and EB isolation and infection were performed as described above and then exposed to physical stress with 1 or 2 min agitation in the bead mill. Bacteria were then infected onto L929 cells at a concentration of $1.00E + 06$ copies/well (MOI = 2:1). The quantity of intracellular bacteria was then determined at 3, 24, 96, 120, 144, and 168 h post-infection by qPCR. *Osmotic stress induced by water treatment*. Quantification of the effect of osmotic shock on Ot viability was performed in the same way as for physical stress except purified bacteria were resuspended in pure water for 5 min prior to infecting host cells. Bacterial copy number after 7 days was quantified by qPCR.

Entry inhibition experiments. IB and EB forms of Ot were isolated from infected host cells as described above. To assess the impact of different interventions on bacterial entry, IB and EB form Ot were added to uninfected L929 or HUVEC cells, labeled with HPG and fixed 3 h post-infection. The number of bacteria inside host cells was counted manually with at least 100 host cells counted for each condition/replicate. To measure the role of clathrin, 0.2 μM siRNA (clathrin, catalog number 4390825 or scramble catalog number 4390843, ThermoFisher Scientific) was added 1 day prior to infection. To measure the effect of perturbing clathrin-mediated endocytosis or macropinocytosis, inhibitors were added for one hour prior to infection and kept in the media during the 3 h of infection. Dynasore hydrate (inhibits endocytosis, catalog number D7693, Sigma) was used at 100 μM, amiloride (inhibit micropinocytosis, 5-(N-Ethyl-N-isopropyl, catalog number A3085, Sigma) at 50 μM and zoniporide hydrochloride hydrate (inhibit micropinocytosis, catalog number SML0076, Sigma) at 100 μM. In order to determine the role of bacterial surface proteins TSA56 and ScaC, IB and EB Ot were added to uninfected host cells at the same time as antibodies against TSA56 and ScaC and the number of intracellular bacteria at three hours post-infection quantified by microscopy.

Statistical analyses. All statistical analyses were carried out using GraphPad Prism version 8.4.3 or 9.2.0. Comparisons between two groups with >10 datapoints per group were carried out using a students unpaired t test, whilst comparisons between two groups with ≤10 datapoints per group were carried out using a

Mann–Whitney test. Comparisons between more than two groups were carried out using one-way ANOVA followed by Dunnetts comparisons. Ns = no significant difference detected, $P > 0.05$; *$P \leq 0.05$; **$P \leq 0.01$; ***$P \leq 0.001$; ****$P \leq 0.0001$. Where results from representative experiments are shown, such as micrographs, the experiment was carried out at least three times.

Reporting summary. Further information on research design is available in the Nature Research Reporting Summary linked to this article.

References

1. Taylor, A., Paris, D. & Newton, P. A systematic review of mortality from untreated scrub typhus (Orientia tsutsugamushi). *PLoS Negl. Trop. Dis.* **9**, e0003971 (2015).
2. Luce-Fedrow, A. et al. A Review of Scrub Typhus (Orientia tsutsugamushi and Related Organisms): Then, Now, and Tomorrow. *Tropical Med. Infect. Dis.* **3**, 8 (2018).
3. McClure, E. et al. Engineering of obligate intracellular bacteria: progress, challenges and paradigms. *Nat. Rev. Microbiol.* https://doi.org/10.1038/nrmicro.2017.59 (2017).
4. Salje, J. Cells within cells: Rickettsiales and the obligate intracellular bacterial lifestyle. *Nat. Rev. Microbiol.* https://doi.org/10.1038/s41579-020-00507-2 (2021).
5. Rikihisa, Y. & Ito, S. Localization of electron-dense tracers during entry of Rickettsia tsutsugamushi into polymorphonuclear leukocytes. *Infect. Immun.* **30**, 231–243 (1980).
6. Lee, J. et al. Fibronectin facilitates the invasion of Orientia tsutsugamushi into host cells through interaction with a 56-kDa type-specific antigen. *J. Infect. Dis.* **198**, 250–257 (2008).
7. Ha, N., Cho, N., Kim, Y., Choi, M. & Kim, I. An autotransporter protein from Orientia tsutsugamushi mediates adherence to nonphagocytic host cells. *Infect. Immun.* **79**, 1718–1727 (2011).
8. Ha, N. et al. Immunization with an Autotransporter Protein of Orientia tsutsugamushi Provides Protective Immunity against Scrub Typhus. *PLoS Negl. Trop. Dis.* **9**, e0003585 (2015).
9. Chu, H. et al. Exploitation of the endocytic pathway by Orientia tsutsugamushi in nonprofessional phagocytes. *Infect. Immun.* **74**, 4246–4253 (2006).
10. Kim, H., Choi, M. & Kim, I. Role of Syndecan-4 in the cellular invasion of Orientia tsutsugamushi. *Micro. Pathog.* **36**, 219–225 (2004).
11. Cho, B., Cho, N., Seong, S., Choi, M. & Kim, I. Intracellular invasion by Orientia tsutsugamushi is mediated by integrin signaling and actin cytoskeleton rearrangements. *Infect. Immun.* **78**, 1915–1923 (2010).
12. Giengkam, S. et al. Improved quantification, propagation, purification and storage of the obligate intracellular human pathogen Orientia tsutsugamushi. *PLoS Negl. Trop. Dis.* **9**, e0004009 (2015).
13. Atwal, S. et al. Evidence for a peptidoglycan-like structure in Orientia tsutsugamushi. *Mol. Microbiol* **105**, 440–452 (2017).
14. Min, C. et al. Genome-based construction of the metabolic pathways of Orientia tsutsugamushi and comparative analysis within the Rickettsiales order. *Comp. Funct. Genom.* **2008**, 623145 (2008).
15. Atwal, S. et al. Clickable methionine as a universal probe for labelling intracellular bacteria. *J. Microbiol. Methods* **169**, 105812 (2020).
16. Hanson, B. Identification and partial characterization of Rickettsia tsutsugamushi major protein immunogens. *Infect. Immun.* **50**, 603–609 (1985).
17. Rikihisa, Y. Anaplasma phagocytophilum and Ehrlichia chaffeensis: subversive manipulators of host cells. *Nat. Rev. Microbio.l* **8**, 328–339 (2010).
18. Elwell, C., Mirrashidi, K. & Engel, J. Chlamydia cell biology and pathogenesis. *Nat. Rev. Microbiol.* **14**, 385–400 (2016).
19. Otten, C., Brilli, M., Vollmer, W., Viollier, P. & Salje, J. Peptidoglycan in obligate intracellular bacteria. *Mol. Microbiol.* **107**, 142–163 (2018).

20. Jacquier, N., Frandi, A., Pillonel, T., Viollier, P. & Greub, G. Cell wall precursors are required to organize the chlamydial division septum. *Nat. Commun.* **5**, 3578 (2014).

21. Irving, S. E., Choudhury, N. R. & Corrigan, R. M. The stringent response and physiological roles of (pp)pGpp in bacteria. *Nat. Rev. Microbiol.* https://doi.org/10.1038/s41579-020-00470-y (2020).

22. Batty, E. M. et al. Long-read whole genome sequencing and comparative analysis of six strains of the human pathogen Orientia tsutsugamushi. *Plos Negl. Trop. Dis.* **12**, e0006566 (2018).

23. Mika-Gospodorz, B. et al. Dual RNA-seq of Orientia tsutsugamushi informs on host-pathogen interactions for this neglected intracellular human pathogen. *Nat. Commun.* **11**, 3363 (2020).

24. Joshi, K. K. & Chien, P. Regulated proteolysis in bacteria: caulobacter. *Annu. Rev. Genet.* **50**, 423–445 (2016).

25. Lamason, R. et al. Rickettsia Sca4 reduces vinculin-mediated intercellular tension to promote spread. *Cell* **167**, 670–683.e610 (2016).

26. Lee, S. Optimal integration of wide field illumination and holographic optical tweezers for multimodal microscopy with ultimate flexibility and versatility. *Opt. Express.* **26**, 8049–8058 (2018).

27. Huang, B., Wang, W., Bates, M. & Zhuang, X. Three-dimensional super-resolution imaging by stochastic optical reconstruction microscopy. *Science* **319**, 810–813 (2008).

28. Wang, Y. et al. Localization events-based sample drift correction for localization microscopy with redundant cross-correlation algorithm. *Opt. Express.* **22**, 15982–15991 (2014).

29. Okuda, S. et al. jPOSTrepo: an international standard data repository for proteomes. *Nucleic Acids Res.* **45**, D1107–D1111 (2017).

Author contributions

S.A., J.W., and S.G. contributed equally to this work and carried out the majority of experiments in this work. S.A. and S.G. carried out multiple experiments throughout the work whilst J.W. performed all proteomics experiments and analysis. K.S. carried out qRT-PCR experiments and Y.J. and S.C. performed Ot growth curve experiments. T.C. and H.H. carried out STORM microscopy experiments, whilst S.H.L. supervised that work and analyzed that data. L.C.W. worked with J.W. on proteomics sample preparation and analysis, whilst RMS supervised the proteomics work and assisted with the analysis. J.S. designed experiments, analyzed data, carried out experiments, and wrote the paper.

Competing interests

The authors declare no competing interests.

Additional information

Supplementary information The online version contains supplementary material available at https://doi.org/10.1038/s41467-022-31176-9.

Correspondence and requests for materials should be addressed to Jeanne Salje.

Peer review information *Nature Communications* thanks David Walker and the other, anonymous, reviewer(s) for their contribution to the peer review of this work.

Reprints and permission information is available at http://www.nature.com/reprints

Publisher's note Springer Nature remains neutral with regard to jurisdictional claims in published maps and institutional affiliations.